Aust. J. Phys., 1996, **49**, 161–82

Diffusion Monte Carlo Study of Electrons in Two-dimensional Layers*

Francesco Rapisarda and Gaetano Senatore

Dipartimento di Fisica Teorica, Università di Trieste,
Strada Costiera 11, I-34014 Trieste, Italy.

Abstract

We investigate the phase diagram of electrons in two dimensions at $T = 0$ by means of accurate diffusion Monte Carlo simulations within the fixed-node approximation. At variance with previous studies, we find that in an isolated layer Slater–Jastrow nodes yield stability of the fully polarised fluid at intermediate coupling, before freezing into a triangular crystal sets in. We have also studied coupled layers of electrons and of electrons and holes. Preliminary results show that at large coupling, as two layers are brought together from infinity, inter-layer correlation first stabilises the crystalline phase at distances of the order of the in-plane inter-particle spacing. As the distance is further decreased the effect of correlation, as expected, turns into an enhanced screening, which disrupts the crystalline order in favour of liquid phases.

1. Introduction

The electron gas, a system of electrons interacting with the $1/r$ potential in the presence of a uniform neutralising background, is one of the simplest models to study the electronic motion in two dimensions. In spite of its simplicity, the system is interesting from many points of view. It is a non-trivial model for many-body theory (Isihara 1989) and has a phase diagram displaying, with lowering the density, transitions to states with magnetic ordering and to the Wigner crystal (Ceperley 1978). In fact, a two dimensional electron gas can be realised at the interface between GaAs and $Al_xGa_{1-x}As$ and at the interface of metal-oxide–semiconductor structures (Ando *et al.* 1982). In past years, systems of electrons confined to two dimensions have attracted a great deal of experimental attention in connection with the quantum Hall effect (von Klitzing *et al.* 1980; Tsui *et al.* 1982), high-temperature superconductivity (Bednorz and Müller 1986; see, e.g., Gupta and Multari 1993), and Wigner crystallisation (Jiang *et al.* 1990; Goldman *et al.* 1990; Williams *et al.* 1991; Pudalov *et al.* 1993). More recently, experiments focussing on the effect of inter-layer correlation on transport have been carried out on coupled layers of two-dimensional carriers, both without (Eiseinstein *et al.* 1992*a*; Sivan *et al.* 1992) and with a magnetic field (Eiseinstein *et al.* 1992*b*, 1995).

* Refereed paper based on a contribution to the Gordon Godfrey Workshop on Atomic and Electron Fluids, held at the University of New South Wales, Sydney, in September 1994.

0004-9506/96/010161$10.00

The phase diagram of the electron gas has received a lot of attention since Wigner (1938) pointed out that at low density electrons would crystallise to minimise the potential energy, while at high density the electronic plasma becomes an ideal Fermi gas with total spin $S = 0$ (normal fluid) to minimise the kinetic energy. In fact, a few years earlier, a suggestion had been made by Bloch (1929) that with decreasing the density the Pauli exclusion principle would make the state with all the spins aligned (polarised fluid) lower in energy than the normal fluid. Somewhat later, Overhauser (1959, 1960, 1962) argued that within an Hartree–Fock treatment states with a spatial modulation of the spin (spin density waves) would be favourable in energy with respect to the normal fluid at all densities. All these considerations, originally made for the electron gas in three dimensions at $T = 0$, are naturally extended to the two-dimensional situation, where all properties of the system are functions of one dimensionless parameter $r_s = 1/\sqrt{\pi n_0} a_B$, with n_0 the average planar density and a_B the Bohr radius. It may be shown that the density parameter r_s also gives a measure of the coupling, expressed as the ratio of potential and kinetic energies.

A first assessment of the phase diagram of the two-dimensional electron gas was made with the variational Monte Carlo (VMC) method by Ceperley (1978), who investigated the competition between normal and polarised fluids and the triangular Wigner crystal. He found that, by lowering the density, the sequence of stable phases was: normal fluid, polarised fluid, Wigner crystal. However, a subsequent study (Tanatar and Ceperley 1989) using the more accurate fixed-node diffusion Monte Carlo (DMC) method gave no evidence for the stability of the polarised fluid, predicting a crystallisation from the normal fluid. Also, a recent VMC investigation of Moroni *et al.* (1993) on spin density waves (SDW) found no evidence of stability for such an inhomogeneous phase, with respect to the fluid phases, at relevant values of r_s.

When two layers of electrons are brought together from infinity, at a distance d comparable to the in-plane inter-particle spacing, correlation between electrons on different layers starts to play an important role (Świerkowski *et al.* 1991; Neilson *et al.* 1993; Zheng and MacDonald 1994), possibly yielding a richer phase diagram. In fact a dielectric approach (Świerkowski *et al.* 1991; Neilson *et al.* 1993), treating correlation within the STLS (Singwi *et al.* 1968) approximation, gives indirect evidence of a stabilisation of modulated phases with respect to the normal fluid. One may naively argue that at large in-plane coupling, as d is reduced from ∞, correlation should first reinforce the stability of charge modulated phases, because of the *Madelung* energy gain. On the contrary, for d smaller than the in-plane spacing $r_s a_B$ and yet in the absence of tunnelling between the layers, inter-layer screening should weaken the intra-layer correlations, yielding to a stabilisation of the fluid phases. This is certainly the case when tunnelling sets in, as the two-layer system becomes closer and closer to a single layer at larger density.

In this paper we present some results of a systematic Monte Carlo investigation of the phase diagram of coupled layers of electrons and of electrons and holes. Being the single layer situation our $d = \infty$ (in practice $d \gg r_s a_B$) limit, we first repeat the single layer calculations for various phases. This preparatory study is additionally motivated by recent fixed-node diffusion Monte Carlo simulations of Kwon *et al.* (1993) on the normal fluid, yielding predictions at variance with

those of Tanatar and Ceperley (1989). We next investigate two coupled layers of electrons and of electrons and holes, at an in-plane coupling $r_s = 30$ and for a few values of d. We restrict our study to the symmetric situation of equal in-plane densities and carrier masses. Using the Rydberg as the unit of energy and the in-plane spacing $a = r_s a_B$ as the unit of length (i.e., $m = \frac{1}{2}$, $\hbar = 1/r_s$, $e^2 = 2/r_s$), the Hamiltonian for a single layer (labelled a) reads

$$H^a = -\frac{1}{r_s^2}\sum_{i=1}^{N}\nabla_i^{a2} + \frac{2}{r_s}\sum_{i<j}^{N}\frac{1}{|\mathbf{r}_i^a - \mathbf{r}_j^a|} + \text{const}\,, \tag{1}$$

where the constant is the term due to the presence of the charged background. Similarly for two *symmetric* layers (labelled a and b) at distance d one has

$$H = H^a + H^b \pm \frac{2}{r_s}\sum_{i=1}^{N}\sum_{j=1}^{N}\frac{1}{\sqrt{|\mathbf{r}_i^a - \mathbf{r}_j^b|^2 + d^2}} + \text{const}'\,, \tag{2}$$

with the new constant accounting for the interaction energy of the particles on one plane with the background on the other plane, and the upper (lower) sign referring respectively to the electron–electron(hole) situation.

The outline of the paper is as follows. In the next section, we briefly review both VMC and fixed-node DMC methods and show the form of our trial functions, emphasising changes necessary for the coupled layers. In Section 3, we present our results for an isolated layer, discuss its phase diagram and compare with previous studies. Finally, in Section 4 we present some preliminary results for the electron–electron and electron–hole coupled layers. In all cases, we give predictions for the energies and for pair correlations, and for the isolated layer we also give spin resolved pair correlations.

2. Monte Carlo Method

In dealing with a quantum many-body system one is faced with the calculation of multidimensional integrals. For N particles in 2 dimensions the calculation of the expectation value of the operator $\hat{O}$, on the wavefunction $\Psi_T(R)$, is given by

$$\langle\hat{O}\rangle = \int dR\Psi_T^*(R)\hat{O}\Psi_T(R) \Big/ \int dR|\Psi_T(R)|^2\,, \tag{3}$$

with R denoting a point in the $2N$-dimensional space of configurations. An efficient technique to evaluate such multidimensional integrals is provided by the Monte Carlo (MC) method (Metropolis *et al.* 1953). The integral in (3) is readily rearranged into the standard form

$$\begin{aligned}\langle\hat{O}\rangle &= \int dR|\Psi_T(R)|^2\frac{1}{\Psi_T(R)}\hat{O}\Psi_T(R) \Big/ \int dR|\Psi_T(R)|^2 \\ &= \int dRP(R)O_L(R)\,,\end{aligned} \tag{5}$$

with the *probability density* $P(R)$ given by

$$P(R) = |\Psi_T(R)|^2 \Big/ \int dR |\Psi_T(R)|^2 , \tag{6}$$

and the *local* operator

$$O_L(R) = \frac{1}{\Psi_T(R)} \hat{O} \Psi_T(R) . \tag{7}$$

According to the Monte Carlo method, one generates a set $\{R\}$ of configurations R_i, sampled from the probability $P(R)$ and evaluates the required integral as

$$\langle \hat{O} \rangle \simeq \frac{1}{M} \sum_{i=1}^{M} O_L(R_i) , \tag{8}$$

with a statistical error that decays as $1/\sqrt{M}$ for large M.

In the VMC method, one assumes a trial wavefunction $\Psi_T(R;\mathbf{a})$, which can be optimised with respect to the variational parameters $\mathbf{a}$, by minimising the expectation value of the energy $E(\mathbf{a}) = \langle \Psi_T(\mathbf{a}) | \hat{H} | \Psi_T(\mathbf{a}) \rangle / \langle \Psi_T(\mathbf{a}) | \Psi_T(\mathbf{a}) \rangle$, or alternatively the energy variance (Umrigar *et al.* 1988). All the integrals required in the calculation of expectation values are calculated using the MC method sketched above. The choice of the wavefunction and the modelling of its variational flexibility are crucial in the VMC method.

One may improve on the variational estimates by resorting to the fixed-node DMC (Reynolds *et al.* 1982; see, also, Umrigar *et al.* 1993). In this method one propagates a trial wavefunction $\Psi_T(R) \equiv \Phi(R,t{=}0)$ in imaginary time t, to project out the higher energy components and filter out the ground state $\Phi_0(R) = \Phi(R, t{=}\infty)$. In fact, for reasons of computational efficiency one introduces the *importance sampling* and works with the *density* $f(R,t) = \Phi(R,t)\Psi_T(R)$. It is easy to show that the Schrödinger equation in imaginary time implies, for a system of N particles, the differential equation

$$\frac{\partial f(R,t)}{\partial t} = \frac{1}{r_s^2} \sum_{i=1}^{N} \nabla_i \cdot (\nabla_i f - f \nabla \ln \Psi_T^2) - (E_L(R) - E_T) f , \tag{9}$$

with the local energy $E_L(R)$ defined according to (7), from the Hamiltonian $\hat{H}$, and E_T a normalisation constant. This equation may be interpreted as a diffusion equation for the probability density f, provided that $f(R,t) \geq 0$, and this may be most easily accomplished by forcing the nodes of $\Phi(R,t)$ to coincide with those of $\Psi_T(R)$. This fixed-node approximation has a variational character (Ceperley 1991) and gives the best energy upper bound consistent with the nodal structure of the trial function.

In practice, in the DMC method, an initial ensemble of configurations $\{R\}$, sampled from the probability density $f(R,0) = \Psi_T^2(R)$, is evolved forward in time by the diffusion equation (9) and reaches the equilibrium distribution at sufficiently large t. Asymptotically, the configurations are sampled according

to the (*mixed*) probability density $f(R,\infty) = \Phi_0(R)\Psi_T(R)$ and can be used to evaluate the *mixed estimator* (Ceperley and Kalos 1979)

$$\langle \hat{O} \rangle_{mix} = \frac{\langle \Psi_T | \hat{O} | \Phi_0 \rangle}{\langle \Psi_T | \Phi_0 \rangle} \simeq \frac{1}{M} \sum_{i=1}^{M} O_L(R_i) \tag{10}$$

of an operator $\hat{O}$. Here $\Phi_0(R)$ is the lowest-energy eigenstate of the Hamiltonian which satisfies the fixed-node boundary condition (i.e., $\Phi_0(R)\Psi_T(R) \geq 0$). Only for operators which commute with the Hamiltonian will the mixed estimator coincide with the ground state expectation value $\langle \Phi_0 | \hat{O} | \Phi_0 \rangle / \langle \Phi_0 | \Phi_0 \rangle$. For other operators, the bias in the mixed estimator is first order in δ, where $|\Phi_0\rangle = |\Psi_T\rangle + \delta|\Psi\rangle$. One can improve by computing the *extrapolated* estimator,

$$\langle \hat{O} \rangle_{ext} = 2\langle \hat{O} \rangle_{mix} - \langle \hat{O} \rangle_{VMC} , \tag{11}$$

with $\langle \hat{O} \rangle_{VMC} = \langle \Psi_T | \hat{O} | \Psi_T \rangle / \langle \Psi_T | \Psi_T \rangle$ the variational estimate. The bias in the extrapolated estimator is second order in δ. Methods to compute unbiased ground state expectation values have been proposed (Liu *et al.* 1974); however they introduce large statistical errors, and in this paper we will use the extrapolated estimator.

In the actual simulation one evolves the discrete representation of the density $f(r,t)$ using a finite time step τ and an approximation for the Green function of the differential equation (9) which is exact only in the limit $\tau \to 0$. This introduces a time step error, which can be either (i) extrapolated out by repeating the simulation with various time steps or (ii) made small by choosing time steps that yield a high acceptance of the MC moves (Reynolds *et al.* 1982). Most of the energies calculated in this work have been obtained with the second procedure, i.e., working at constant acceptance (typically of $\simeq 99 \cdot 94\%$) to conform with the prescription of Kwon *et al.* (1993) (see also Kwon 1994). However, for the single layer, we have also performed extrapolations to $\tau = 0$ (see below). For the structural properties, on the other hand, we always report results for fixed acceptance, since statistical noise tends to be larger than the time step bias. The time step error can be avoided altogether by using the Green Function Monte Carlo method (Ceperley and Kalos 1979).

Because of the finite number N of particles used, simulations yield predictions that are affected by size effects. For charged fermions they are particularly severe, both in the kinetic and potential energies (Ceperley 1978). Even using numbers of particles N corresponding to closed shells of one-particle orbitals and performing the Ewald summation of the interactions on the infinite periodic replicas of the simulation box, residual size effects need to be extrapolated out. In practice, one assumes (Ceperley 1978) that the N dependence of the energy is the same for VMC and DMC and performs simulations yielding VMC energies and their size dependence. Thus one may perform the more costly DMC simulations only for one value of N and extrapolate the DMC energy to the bulk limit using the VMC information. Tanatar and Ceperley (1989) checked the assumption above in selected cases and found that indeed the number dependence of VMC and DMC energies was the same within statistical error.

3. Trial Wavefunctions

In the present investigation, the primary role of the trial wavefunction Ψ_T is (i) to provide the nodes to use in the DMC simulations and (ii) to yield the VMC energies and their N dependence. The simplest choice of trial function for a single layer with $N = N_\downarrow + N_\uparrow$ electrons is of the Slater–Jastrow (SJ) type

$$\Psi_T(R) = D_\downarrow(\phi_{nm}) D_\uparrow(\phi_{nm}) \exp\left(-\tfrac{1}{2} \sum_{i \neq j}^{N} u(r_{ij}) \right), \tag{12}$$

where the determinant $D_\downarrow$ ($D_\uparrow$) is constructed with the $N_\downarrow$ ($N_\uparrow$) one-particle orbitals $\phi_n(\mathbf{r}_m) \equiv \phi_{nm}$ that are lowest in energy and $u(r)$ is a suitable two-body pseudopotential. The form of the orbitals depends on the phase under investigation, a natural choice being plane waves for the fluid phases and localised gaussians for the crystal. Improved trial functions (BF3) including backflow, as well as three-body terms in the Jastrow exponential, have been recently used to study the normal phase of the 2-dimensional electron gas (Kwon *et al.* 1993). They yield some improvement on the SJ trial function, but are computationally more demanding. In view of the very large number of simulations necessary to build a phase diagram, here we choose to work with the simpler SJ functions.

For the two-body pseudopotential $u(r)$ we use in the fluid phases the form that minimises $\langle \Psi_T | H | \Psi_T \rangle / \langle \Psi_T | \Psi_T \rangle$ in the random-phase approximation (RPA) (Gaskell 1961; Ceperley, 1978) and which turns out to be nearly optimal in VMC simulations (Ceperley 1978)

$$2n_0 u(k) = -\frac{1}{S_0(k)} + \sqrt{\frac{1}{S_0^2(k)} + \frac{8r_s}{k^3}}\,. \tag{13}$$

Above, $S_0(k)$ is the static structure factor of non-interacting fermions

$$S_0(k) = \frac{2}{\pi}\left[\sin^{-1} y + y\sqrt{1-y^2} \right], \tag{14}$$

with $y = k/2k_F$ and k_F the Fermi wavevector. This pseudopotential is known to reproduce (Ceperley 1978) the cusp condition for particles with unlike spin projection

$$\lim_{r \to 0} \frac{du(r)}{dr} = -r_s\,, \tag{15}$$

as well as the long-range behaviour necessary for the correct plasmon dispersion

$$\lim_{r \to \infty} u(r) = 1 \cdot 48\sqrt{r_s/r}\,. \tag{16}$$

In the crystalline phase a similar pseudopotential was shown to be nearly optimal (Ceperley 1978),

$$2n_0 u(k) = -1 - \frac{4}{(kl)^2} + \sqrt{1 + \frac{8}{(kl)^2} + \frac{8r_s}{k^3}}\,, \tag{17}$$

with $l = l(r_s)$ the localisation length of the gaussian orbital $\phi(r) \propto \exp(-(r/l)^2)$ centred at the sites of the chosen lattice.

The above SJ trial functions for a single layer are easily generalised to the case of two coupled layers (a and b),

$$\Psi_T(R) = D_{a\downarrow}(\phi_{nm}) D_{a\uparrow}(\phi_{nm}) D_{b\downarrow}(\phi_{nm}) D_{b\uparrow}(\phi_{nm}) \times \exp\left(-\tfrac{1}{2} \sum_{\alpha,\beta=a}^{b} \sum_{i,j}^{N} u_{\alpha\beta}(|\mathbf{r}_i^\alpha - \mathbf{r}_j^\beta|) \right), \tag{18}$$

with the second sum excluding the term with $i = j$ when $\alpha = \beta$, and $D_{\alpha\sigma}$ a determinant of single particle orbitals for the particle with spin projection σ on the layer α. We have obtained the two-body pseudopotentials $u_{\alpha\beta}(r)$ by a straightforward generalisation of Ceperley's (1978) approach. For the fluid phases we get

$$2n_0 u_{\alpha\beta}(k) = -\frac{\delta_{\alpha\beta}}{S_0(k)} + \tfrac{1}{2}\left(\sqrt{\frac{1}{S_0^2(k)} + V_+(k)} + (2\delta_{\alpha\beta} - 1) \sqrt{\frac{1}{S_0^2(k)} + V_-(k)} \right), \tag{19}$$

and for the crystal

$$2n_0 u_{\alpha\beta}(k) = -\delta_{\alpha\beta}\left(-1 - \frac{4}{(kl)^2} \right) + \tfrac{1}{2}\left(\sqrt{1 + \frac{8}{(kl)^2} + V_+(k)} + (2\delta_{\alpha\beta} - 1) \sqrt{1 + \frac{8}{(kl)^2} + V_-(k)} \right), \tag{20}$$

where

$$V_\pm(k) = \frac{8r_s}{k^3}[1 \pm \exp(-kd)], \tag{21}$$

with the upper (lower) sign referring to electron–electron (hole) coupled layers at distance d.

We note that the above formulae for two layers are restricted to the symmetric case, which is the only one that will be considered here, and to situations in which the in-layer motion of the fermions is strictly two-dimensional and inter-layer tunneling may be neglected. For the electron–hole situation we find that the above inter-layer pseudopotential $u_{ab}(r)$ may become poor for strong inter-layer couplings. In such a case we augment it with a short range attraction, which we expand in cosines with coefficients that are determined variationally. More details of the coupled layers study will be given elsewhere (Rapisarda and Senatore 1996). Here we stress that optimal pseudopotentials are of primary importance for the reliability of extrapolated estimates according to (11), in that they bring Ψ_T closest to Φ_0.

4. The 2-dimensional Electron Gas

(4a) Ground State Energies and Phase Diagram

We have performed Monte Carlo simulations of the 2-d electrons gas for three different phases and for several values of the coupling constant r_s. In all cases we have used SJ trial functions, as briefly summarised above. To the best of our knowledge, the ingredients of our calculations are equivalent to those of similar calculations carried out by Tanatar and Ceperley (1989) and by Kwon *et al.* (1993) and we would expect our results to coincide with those of these previous studies, within statistical errors. This is indeed the case when we compare our energies with the SJ results of Kwon *et al.* that is for the normal fluid at $r_s = 5, 10, 20$. However, the same is not true for the comparison with the results of Tanatar and Ceperley, in which case we have to record significant discrepancies, largely outside the error bars. This is quite evident from Tables 1–3, where all our energies, variational and diffusion, have been collected, together with the diffusion results of Tanatar and Ceperley. We find that their total energies are always below ours for the normal fluid and always above for the polarised fluid and the triangular crystal, with the exception of the polarised fluid at $r_s = 30$ where they agree within error bars. We have no explanation for these discrepancies and we may only stress that our results do agree with the more recent study of Kwon *et al.*

Table 1. Size dependence of the Slater–Jastrow VMC energy (in Ry) of the normal electron liquid at $5 \leq r_s \leq 40$ and χ^2 parameters

Fixed-node DMC total energies for $N = 58$ and in the bulk limit are shown and compared with the results of Tanatar and Ceperley (1989) [in square brackets]. Also, the correlation energy E_c is given, together with the kinetic $\langle T \rangle$ and potential energies $\langle V \rangle$, as obtained from our fit to the correlation energy

	$r_s = 5{\cdot}0$	$r_s = 10{\cdot}0$	$r_s = 20{\cdot}0$	$r_s = 30{\cdot}0$	$r_s = 40{\cdot}0$
$N = 26$	−0·29356(8)	−0·16851(3)	−0·09173(1)	−0·063346(6)	−0·048479(4)
$N = 42$	−0·29596(5)	−0·16897(2)	−0·091802(9)	−0·063345(5)	−0·048477(3)
$N = 58$	−0·29357(5)	−0·16837(2)	−0·091651(9)	−0·063283(5)	−0·048442(3)
$N = 74$	−0·29446(5)	−0·16856(2)	−0·091677(8)	−0·063291(4)	−0·048446(3)
$N = 114$	−0·29374(5)	−0·16837(2)	−0·091601(8)	−0·063257(6)	−0·048426(3)
E_∞^{VMC}	−0·29351(6)	−0·16826(2)	−0·091558(9)	−0·063230(6)	−0·048410(3)
b_1	0·043(1)	0·0099(4)	0·0024(2)	0·0008(1)	0·00044(7)
b_2	−0·046(3)	−0·017(1)	−0·0071(4)	−0·0038(3)	−0·0023(2)
χ^2	3·66	2·35	1·69	0·53	0·54
E_{58}^{DMC}	−0·2980(1)	−0·17036(2)	−0·09248(1)	−0·063792(8)	−0·048813(4)
	[−0·2998(1)]	[−0·17105(8)]	[−0·09273(2)]	[−0·063934(7)]	
E_∞^{DMC}	−0·2979(2)	−0·17023(4)	−0·09240(2)	−0·06374(1)	−0·048780(9)
	[−0·2996(1)]	[−0·17089(9)]	[−0·09268(2)]	[−0·06392(1)]	
$\langle T \rangle$	0·0745	0·02513	0·00875	0·00480	0·003159
$\langle V \rangle$	−0·3724	−0·19537	−0·10115	−0·06855	−0·051940
E_c	−0·0978(2)	−0·06019(4)	−0·03488(2)	−0·02485(1)	−0·019394(9)
	[−0·0955(1)]	[−0·06085(9)]	[−0·03516(2)]	[−0·02502(1)]	

The fixed-node DMC results given in Tables 1–3 have all been obtained with simulations at a fixed acceptance of about 99·94%. This is accomplished by carefully tuning the time step at each r_s, between $\tau = 0{\cdot}06\ \mathrm{Ry}^{-1}$ for $r_s = 5$ and $\tau = 6{\cdot}6\ \mathrm{Ry}^{-1}$ for $r_s = 75$. We have also performed linear extrapolations to $\tau = 0$,

to ascertain the systematic bias introduced by the use of a small but finite time step. In Fig. 1 we show a typical extrapolation. Similar fits are obtained for all the cases studied. We find that the overall effect of extrapolation to $\tau = 0$ is a rigid downward shift of $r_s^{3/2}E(r_s)$ by an amount of the order of a couple of mRy.

Table 2. Size dependence of the Slater–Jastrow VMC energy (in Ry) of the fully polarised electron liquid at $5 \leq r_s \leq 75$ and χ^2 parameters

Fixed-node DMC total energies for $N = 57$ and in the bulk limit are shown and compared with the results of Tanatar and Ceperley (1989) [in square brackets]. Also, the correlation energy E_c is given, together with the kinetic $\langle T \rangle$ and potential energies $\langle V \rangle$, as obtained from our fit to the correlation energy (equation 28)

	$r_s = 5{\cdot}0$	$r_s = 10{\cdot}0$	$r_s = 20{\cdot}0$	$r_s = 30{\cdot}0$	$r_s = 40{\cdot}0$	$r_s = 75{\cdot}0$
$N = 21$	−0·28958(7)	−0·16965(2)	−0·092584(8)	−0·063880(6)	−0·048851(4)	−0·026912(1)
$N = 37$	−0·28603(9)	−0·16855(3)	−0·09222(1)	−0·063687(5)	−0·048727(3)	−0·026868(2)
$N = 57$	−0·28401(8)	−0·16793(3)	−0·092025(9)	−0·063590(5)	−0·048670(3)	−0·026850(1)
$N = 69$	−0·28529(7)	−0·16833(3)	−0·092136(7)	−0·063650(5)	−0·048697(2)	−0·026857(1)
$N = 113$	−0·28401(7)	−0·16792(2)	−0·092004(7)	−0·063574(4)	−0·048657(2)	−0·026845(1)
E_∞^{VMC}	−0·28374(9)	−0·16785(3)	−0·09197(1)	−0·063558(6)	−0·048639(3)	−0·026836(1)
b_1	0·055(3)	0·017(1)	0·0050(3)	0·0026(2)	0·0014(1)	0·00041(4)
b_2	−0·050(6)	−0·015(2)	−0·0064(6)	−0·0033(4)	−0·0025(2)	−0·00103(8)
χ^2	0·27	0·13	0·46	3·31	4·13	4·77
E_{57}^{DMC}	−0·2869(1)	−0·16902(2)	−0·09246(1)	−0·063854(4)	−0·048865(4)	−0·026960(1)
	[−0·28581(9)]	[−0·16853(5)]	[−0·09237(2)]	[−0·063826(8)]	[−0·048841(2)]	[−0·026947(3)]
E_∞^{DMC}	−0·2866(2)	−0·16895(7)	−0·09240(2)	−0·06383(1)	−0·048843(9)	−0·026947(3)
	[−0·2858(2)]	[−0·16807(9)]	[−0·09223(2)]	[−0·06379(1)]	[−0·048844(7)]	[−0·026932(3)]
$\langle T \rangle$	0·0951	0·02846	0·00920	0·00488	0·003134	0·001210
$\langle V \rangle$	−0·3817	−0·19739	−0·10161	−0·06870	−0·051978	−0·028157
E_c	−0·0271(2)	−0·01918(7)	−0·01252(2)	−0·00945(1)	−0·007652(9)	−0·004667(3)
	[−0·0263(2)]	[−0·0183(1)]	[−0·0123(2)]	[−0·00942(1)]	[−0·007653(7)]	[−0·004652(3)]

Table 3. Size dependence of the Slater–Jastrow VMC energy (in Ry) of the triangular electron crystal at $20 \leq r_s \leq 75$ and χ^2 parameters

Fixed-node DMC total energies for $N = 56$ and in the bulk limit are shown and compared with the results of Tanatar and Ceperley (1989) [in square brackets]

	$r_s = 20{\cdot}0$	$r_s = 30{\cdot}0$	$r_s = 40{\cdot}0$	$r_s = 50{\cdot}0$	$r_s = 75{\cdot}0$
$N = 16$	−0·092154(9)	−0·063753(5)	−0·048836(3)	−0·039631(2)	−0·026992(1)
$N = 30$	−0·091974(8)	−0·063653(4)	−0·048768(3)	−0·039580(1)	−0·026963(1)
$N = 56$	−0·091904(6)	−0·063613(3)	−0·048738(2)	−0·039560(1)	−0·026953(1)
$N = 80$	−0·091897(6)	−0·063600(3)	−0·048727(2)	−0·039556(1)	−0·026949(1)
$N = 120$	−0·091888(6)	−0·063592(3)	−0·048727(2)	−0·039553(1)	−0·026947(1)
E_∞^{VMC}	−0·091869(4)	−0·063585(2)	−0·048720(1)	−0·0395484(7)	−0·0269450(6)
c	−0·0180(7)	−0·0108(4)	−0·0075(2)	−0·0052(1)	−0·00300(8)
χ^2	3·26	0·96	4·07	1·48	0·89
E_{56}^{DMC}	−0·092376(8)	−0·063846(5)	−0·048878(2)	−0·039646(2)	−0·026993(1)
		[−0·063778(5)]	[−0·0488863(5)]	[−0·039621(3)]	[−0·026988(1)]
E_∞^{DMC}	−0·09233(1)	−0·063820(6)	−0·048860(2)	−0·039634(2)	−0·026986(1)
		[−0·063760(9)]	[−0·048852(6)]	[−0·039613(5)]	[−0·026981(2)]

As we have already mentioned, simulations are made at finite number N of particles and results need to be extrapolated to the bulk limit. In Tables 1–3 we have recorded our variational energy for N ranging between 16 and 120. For the fluid phases, the extrapolation to $N = \infty$ is made according to a scheme due

to Tanatar and Ceperley (1989), through the following ansatz for the energy per particle

$$E_N = E_\infty + b_1(r_s)\Delta T_N + \frac{b_2(r_s)}{N}, \tag{22}$$

where ΔT_N is the kinetic energy difference between a system with N electrons and one in the bulk limit (i.e., $N = \infty$), for non-interacting electrons at $r_s = 1$. We determine the variational parameters E_∞, b_1, and b_2 by a least squares fit of our variational energies. To extrapolate the DMC energies we assume with Ceperley (1978) that the difference $E_N - E_\infty$ is the same for VMC and DMC, being given by the last two terms on the rhs of (22). We proceed in a similar manner for the crystalline phase by resorting to the ansatz (Tanatar and Ceperley 1989)

$$E_N = E_\infty + \frac{c(r_s)}{N^{\frac{3}{2}}}. \tag{23}$$

All the extrapolated energies listed in Tables 1–3 have been obtained with these procedures and we also give in the same tables details of the fits.

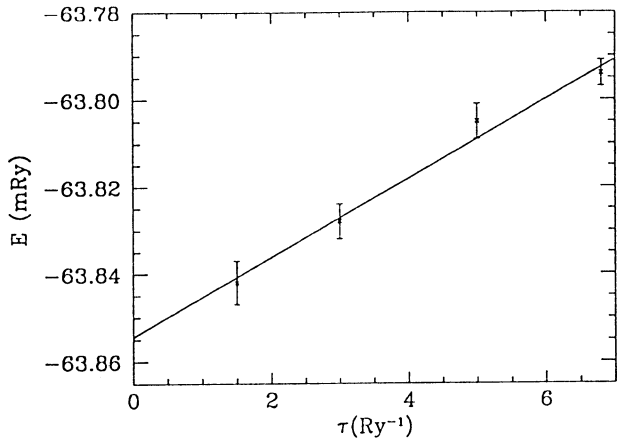

Fig. 1. Extrapolation to $\tau = 0$ for the total energy $E_\tau = E_0 + \alpha\tau$ in the 2-dimensional electron gas, for the fully polarised fluid at $r_s = 30$ and $N = 57$. Here $E_0 = -0{\cdot}063857(4)$ Ry, $\alpha = 9{\cdot}6 \times 10^{-6}$ Ry^2, with a $\chi^2 = 1{\cdot}73$.

The present results for the energies of the electron gas are the most accurate to date covering normal and polarised fluids, as well as the triangular crystal, over a large range of densities. Therefore we have fitted our extrapolated DMC energies to analytic expressions, one for the fluid phases and one for the crystal. For the crystal we have used the same form as Tanatar and Ceperley (1989)

$$E(r_s) = \frac{c_1}{r_s} + \frac{c_2}{r_s^{\frac{3}{2}}} + \frac{c_2}{r_s^2}. \tag{24}$$

The resulting coefficients are shown in Table 4.

Table 4. Parameters of the approximant of (28) to the correlation energy of normal and polarised electron liquids, and of (27) to the total energy of the triangular crystal, determined by a nonlinear fit

The resulting χ^2 values are also shown. Here a_0 and c_1 are in Ry

	a_0	a_1	a_2	a_3	χ^2
Normal fluid	−0·3850	7·3218	0·16008	3·1698	0·09
Polarised fluid	−0·062217	4·4469	0·93426	8·0116	0·62
Crystal	c_1	$c_{\frac{3}{2}}$	c_2	χ^2	
	−2·20943	1·58948	0·146762	2·55	

To fit the fluid energies we have chosen to use an approximant for the correlation energy different from the one used in previous studies, in order to reproduce the structure of the small r_s expansion up to the first two leading terms (see e.g. Isihara 1989),

$$E_c(r_s) = -0{\cdot}3850 - 0{\cdot}1726 r_s \ln r_s + \cdots, \quad r_s \to 0. \tag{25}$$

Previous fits were short of the logarithmic term present in (25). Here $E_c = E - E_{HF}$ denotes the correlation energy per particle (in Ry) and the Hartree–Fock energy is given by

$$E_{HF} = \frac{1+\xi^2}{r_s^2} - \frac{4\sqrt{2}}{3\pi r_s}[(1+\xi)^{\frac{3}{2}} + (1-\xi)^{\frac{3}{2}}], \tag{26}$$

for a system with spin polarisation ξ $(0 \le \xi \le 1)$. We shall show below that the present fit, which was inspired by similar work of Vosko *et al.* (1980) on the 3-dimensional electron gas, appears to be superior to the one previously employed.

We start by noting that the choice

$$r_s^2 \frac{d}{dr_s}\left(\frac{E_c}{r_s}\right) = -a_0 \frac{1+b_1 x}{1+b_1 x + b_2 x^2 + b_3 x^3}, \tag{27}$$

with $x = \sqrt{r_s}$, admits the structure of (25) for small r_s, as well as reproducing the structure of the crystal expansion of (24) for large r_s. Assuming that the denominator on the rhs of (27) has a real root for negative values of x and two complex roots, one obtains after some algebra, in terms of the four parameters a_0, a_1, a_2, a_3,

$$E_c(r_s) = a_0\left\{1 + Ax^2\left[B \ln \frac{x+a_1}{x} + C \ln \frac{\sqrt{x^2+2a_2x+a_3}}{x} + D\left(\tan^{-1}\frac{x+a_2}{\sqrt{a_3-a_2^2}} - \frac{\pi}{2}\right)\right]\right\}, \tag{28}$$

where

$$A = \frac{2(a_1 + 2a_2)}{2a_1a_2 - a_3 - a_1^2}, \quad B = \frac{1}{a_1} - \frac{1}{a_1 + 2a_2}, \quad C = \frac{a_1}{a_3} - \frac{2a_2}{a_3} + \frac{1}{a_1 + 2a_2},$$

$$D = \frac{F - a_2 C}{\sqrt{a_3 - a_2^2}}, \quad F = 1 + (2a_2 - a_1)\left(\frac{1}{a_1 + 2a_2} - \frac{2a_2}{a_3}\right). \tag{29}$$

Also, the parameters b_1, b_2, b_3 appearing in (27) are related to a_1, a_2, a_3 by

$$b_1 = \frac{1}{a_1} + \frac{2a_2}{a_3}, \quad b_2 = \frac{1}{a_3} + \frac{2a_2}{a_1 a_3}, \quad b_3 = \frac{1}{a_1 a_3}. \tag{30}$$

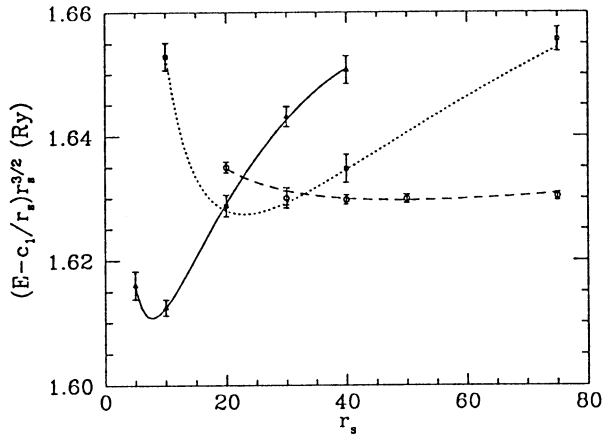

Fig. 2. Ground state energy of the electron gas in 2 dimensions as function of the coupling r_s, calculated by SJ fixed-node DMC. The DMC energies of the normal fluid, polarised fluid and triangular crystal are given by the triangles, squares and circles, respectively. We have subtracted the Madelung energy $-2 \cdot 2122/r_s$ and multiplied by $r_s^{3/2}$. The curves are fits to the DMC points as explained in the text.

In Table 4 we report the coefficients of the fits of the correlation energy for both normal and fully polarised fluids. One can see from the small values of the χ^2 that the chosen approximant works really well. In fact from Fig. 2, where the energies are shown in an expanded scale, it is clear that for the fluid phases the fitting curves go through the calculated points within fractions of error bars, though these are extremely small. For the normal fluid the relative discrepancy between calculated correlation energies and fit predictions are always less than 3×10^{-4}, while for the polarised phase they are always less than 2×10^{-3}. We note that for the normal fluid we have fixed $a_0 = -0 \cdot 3850$ according to the small r_s expansion. Had we treated it as a free parameter we would get similar parameters and χ^2, with $a_0 = E_c(r_s{=}0)$ about 1% below the exact value. For the polarised fluid, in fact, we treated a_0, which is not known, as a free parameter obtaining $a_0 = -0 \cdot 06222$. It would be interesting to determine the exact value of $E_c(r_s{=}0)$ for the polarised fluid, to further assess the quality of the present fitting scheme.

We have also fitted our correlation energy to the Padé approximant proposed by Tanatar and Ceperley (1989) and also used by Kwon *et al.* (1993). In such a fit one has also four parameters, with the first, say a_0, satisfying $a_0 = E_c(r_s{=}0)$. We find that fixing $a_0 = -0{\cdot}3850$, a $\chi^2 = 2{\cdot}43$ is obtained, which is satisfactory, though larger than $\chi^2 = 0{\cdot}17$ found with our approximant. However, if a_0 is considered as a free parameter one finds $\chi^2 = 0{\cdot}58$ and $a_0 = E_c(r_s{=}0) = -0{\cdot}3246$, which is about 16% off the exact high density value. We may conclude that our fit is more accurate that the previous one. In fact we find overall that it gives a better account of our data as well as of the limiting behaviour of the correlation energy both at small and large densities.

A knowledge of the correlation energy as an analytic function of r_s, together with the virial theorem for the electron gas (see e.g. March 1958),

$$2\langle T\rangle + \langle V\rangle = -r_s \frac{dE}{dr_s}, \tag{31}$$

with $\langle T\rangle$ and $\langle V\rangle$ the kinetic and potential energy per electron, allows the determination of $\langle T\rangle$ and $\langle V\rangle$. In fact, using $E = \langle T\rangle + \langle V\rangle$, one immediately gets

$$\langle T\rangle = -\frac{d(r_s E)}{dr_s}, \quad \langle V\rangle = \frac{1}{r_s}\frac{d(r_s^2 E)}{dr_s}. \tag{32}$$

In Tables 1–3, we have also reported $\langle T\rangle$ and $\langle V\rangle$ calculated from (32) and our fit of (28). One can easily check that the overall energy gain induced by correlation involves an increase of the kinetic energy and a lowering of the potential energy, with respect to their Hartree–Fock values (see e.g. equation 26). The fractional changes of these two quantities in fact increase with the coupling r_s. In the normal fluid, for instance, $\langle T\rangle/\langle T\rangle_{HF}$ goes from $1{\cdot}86$ to $5{\cdot}07$ in going from $r_s = 5$ to $r_s = 40$, and $\langle V\rangle/\langle V\rangle_{HF}$ from $1{\cdot}55$ to $1{\cdot}73$. Similar though somewhat smaller changes are found in the polarised fluid.

In Fig. 2 we compare our DMC energies for the three phases that we have studied over a range of r_s values from 5 to 75. We find as expected that the normal fluid is stable at high density (i.e., small r_s) and up to $r_s = 20 \pm 2$. However, between $r_s = 20$ and $r_s = 34$ our Slater–Jastrow fixed-node DMC simulations predict the stability of the polarised fluid. This is qualitatively in accord with the early conjecture of Bloch (1929) and the VMC study of Ceperley (1978), while it is at variance with the results of Tanatar and Ceperley (1989), who found that the fully polarised fluid would never be stable and crystallisation would take place at $r_s = 37 \pm 5$ from the normal fluid. Our simulations yield crystallisation into a triangular lattice at $r_s = 34 \pm 4$, which is in accord with the previous estimate of Tanatar and Ceperley.

We should remind the reader that the phase diagram shown in Fig. 2 was obtained employing SJ trial functions and the fixed-node approximation. As we have mentioned above, Kwon *et al.* (1993) have investigated the normal fluid for $r_s \leq 20$ with improved nodes (BF3), finding energies that are a bit lower than the SJ ones. It is tempting to speculate what the phase diagram would look like if all phases were treated with BF3 nodes. One may conjecture, as it appears likely, that the BF3 wavefunctions would yield much smaller changes for the polarised

fluid and the crystal, since these phases are much more constrained than the normal fluid. If this is the case, we anticipate that the range of stability for the polarised fluid should shrink and possibly disappear, with crystallisation in fact taking place from the normal fluid at a coupling of $r_s \approx 35$. That backflow effects are almost negligible in the polarised fluid has been recently demonstrated for ^{3}He by Moroni *et al.* (1995).

(4b) Spin Correlations

Structural properties of the 2-dimensional electron gas have been studied before (Tanatar and Ceperley 1989; Kwon *et al.* 1993), but were restricted to number–number correlations. Here, we have sampled not only the number–number pair correlation function

$$g(r) = \frac{1}{Nn_0} \sum_{i \neq j} \langle \delta(|\mathbf{r}_i - \mathbf{r}_j - \mathbf{r})| \rangle \,, \tag{33}$$

but also its two independent spin components in the normal phase, namely

$$g_{\uparrow\uparrow}(r) = \frac{4}{Nn_0} \sum_{i \neq j=1}^{N/2} \langle \delta(|\mathbf{r}_i - \mathbf{r}_j - \mathbf{r})| \rangle \,, \tag{34}$$

$$g_{\uparrow\downarrow}(r) = \frac{4}{Nn_0} \sum_{i=1}^{N/2} \sum_{j=N/2+1}^{N} \langle \delta(|\mathbf{r}_i - \mathbf{r}_j - \mathbf{r})| \rangle \,. \tag{35}$$

Above, particles 1 to $N/2$ have spin up, particles $N/2+1$ to N have spin down, and as is known $g(r) = (\frac{1}{2})[g_{\uparrow\uparrow}(r) + g_{\uparrow\downarrow}(r)]$. Since the operators whose average yields the pair correlations do not commute with the Hamiltonian, one has to resort to extrapolated averages, according to (11). Thus using (33) and (34) one constructs independently VMC and DMC pair correlations, and from these the extrapolated estimator $g(r) \equiv g_{ext}(r) = 2g_{mix}(r) - g_{VMC}(r)$.

In Fig. 3 we show the pair correlation function $g(r)$ for the various couplings that we have studied. Where comparison is possible, we find that our results are in agreement with the predictions of Tanatar and Ceperley (1989), while minor differences exist with the results of Kwon *et al.* who used different trial functions.

In Fig. 4 we compare $g(r)$, $g_{\uparrow\downarrow}(r)$, and $g_{\uparrow\uparrow}(r)$, at $r_s = 5$ and $r_s = 40$, the largest and the smallest densities that we have studied. Clearly the $g_{\uparrow\uparrow}(r)$ has a much smaller peak than the $g_{\uparrow\downarrow}(r)$, and this is immediately traced to the Pauli exclusion principle, which discourages the close approach of like spins pairs. We find that with increasing the coupling all functions become more structured, but also qualitative changes take place. At high density, one observes an alternation of shells of down and up spins (around a given up spin). The effect is small but clearly discernible. As the density is lowered, however, and the coupling becomes more important, the location and coordination of down and up spin shells tend to coincide. The first peak of $g_{\uparrow\downarrow}(r)$, though, remains much higher than the corresponding peak in $g_{\uparrow\uparrow}(r)$.

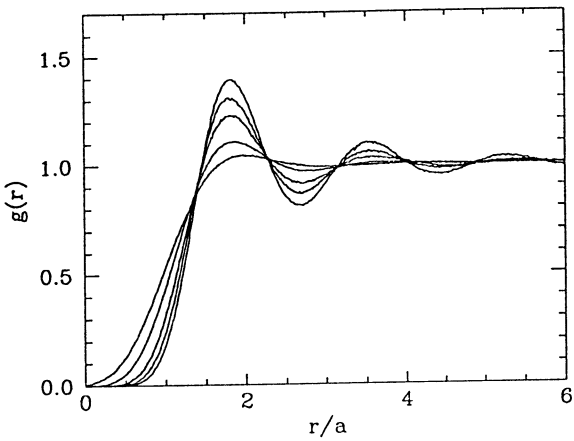

Fig. 3. Extrapolated pair correlation function $g(r)$ of the normal electron liquid at $r_s = 5, 10, 20, 30, 40$, calculated by SJ fixed-node DMC simulations. Curves with increasing peak height refer to increasing values of r_s.

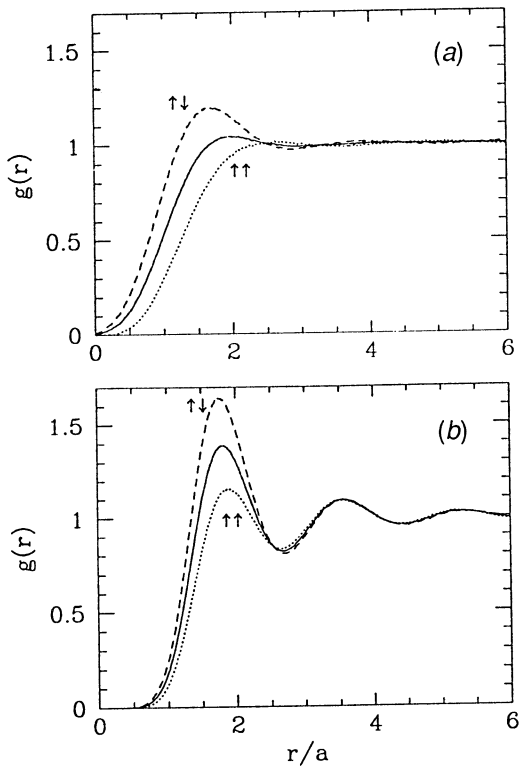

Fig. 4. Comparison of the number–number, up–down, and up–up pair correlation functions of the normal electron liquid at (*a*) $r_s = 5$ and (*b*) $r_s = 40$, as calculated by SJ fixed-node DMC simulations. Full, dashed, and dotted curves give respectively $g(r)$, $g_{\uparrow\downarrow}(r)$, and $g_{\uparrow\uparrow}(r)$.

5. Preliminary Results on Coupled Layers

(5a) Energetics

Quite generally, when two neutralised layers of electrons are brought together from infinity there is an energy gain due to the correlated motion of the electrons in the two layers. Though there is similarity with the (van der Waals) problem of the forces between two neutral atoms, there is also a substantial difference due to the planar geometry. For two neutral atoms the interaction energy decays as an inverse power of the distance d, whereas for two planes we expect it to decay with an exponential law. Thus we expect all relevant effects to take place when $d \lesssim r_s a_B$. To illustrate the point above we report in Fig. 5 the potential energy of two (classic) static crystals of electrons as a function of the inter-layer distance, at $r_s = 30$. As expected the energy is remarkably flat for $d \gtrsim r_s a_B$. Calculations were made with the standard Ewald technique (see e.g. Ceperley 1978).

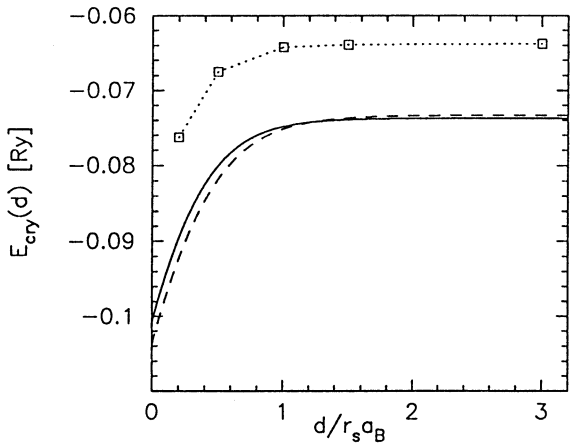

Fig. 5. Ground state energy of coupled crystalline electron layers at $r_s = 30$, as a function of the inter-layer spacing d. The full and dashed curves give the potential (Madelung) energy of respectively two static triangular crystals and two static square crystals, both in AB stacking (see text). The squares are DMC energies of two triangular crystals, with the dotted line a guide to the eye.

We have in fact considered two situations. In the first two triangular crystals are positioned one above the other at distance d in an AB stacking, i.e., with a relative in-plane translation of $(\mathbf{a}_1 + \mathbf{a}_2)/3$, where $\mathbf{a}_1$ and $\mathbf{a}_2$ are the primitive vectors of the triangular lattice. Similarly, we have considered two square crystals in an AB stacking, i.e., with a relative in-plane translation of $(\mathbf{a}_1 + \mathbf{a}_2)/2$, and $\mathbf{a}_1$ and $\mathbf{a}_2$ the primitive vectors of the square lattice. It is worth noting that the coupled triangular arrangement is stable with respect to the coupled square crystals only for $d \gtrsim r_s a_B$, where one recovers the isolated layer energetics, favouring triangular over square crystal (see e.g. Bonsall and Maradudin 1977). For smaller distances the reverse is true, with the square arrangement being lower in energy. Eventually, for $d = 0$ one has a single layer and therefore the triangular lattice will again win. A competition

of this kind has been recently noted by Zheng and Fertig (1995), in Hartree–Fock calculations for coupled crystalline electron layers in the Hall regime, i.e., with an applied magnetic field. We also report, in Fig. 5, the energy of two coupled triangular crystals of electrons in the fully degenerate regime, for comparison. There appears to be an almost rigid upward shift in energy, with respect to the static crystal. This is mostly due to the kinetic energy cost of localising electrons as well as to the increase in Hartree energy in going from point to smeared charges.

Before discussing the DMC results that we have obtained for the phase diagram of coupled electron layers, we should emphasise the importance of working with optimal pseudopotentials, to obtain accurate extrapolated estimates, as well as to reduce statistical errors on the DMC energy estimates for fixed run length. The details of our fixed node DMC simulations for coupled layers are similar to those of the isolated layer. In particular we have worked at a fixed acceptance of about 99·94% and for the energies we have performed extrapolation to the bulk limit, using the same formulae as in the preceding section. In Table 5 we give, as an example, the size dependence of coupled layers at $d = 0{\cdot}5 r_s a_B$ and $r_s = 30$.

Table 5. Size dependence of the Slater–Jastrow VMC energy (in Ry) of two coupled electron layers at $r_s = 30$ and $d = 0{\cdot}5 r_s a_B$, with χ^2 parameters

Fixed-node DMC total energies for finite N and in the bulk limit are also shown

	Normal fluid		Polarised fluid		Triangular crystal
$N = 26$	−0·066322(6)	$N = 21$	−0·066627(7)	$N = 16$	−0·066630(6)
$N = 42$	−0·066353(5)	$N = 37$	−0·066464(6)	$N = 30$	−0·066566(5)
$N = 58$	−0·066283(5)	$N = 57$	−0·066378(5)	$N = 56$	−0·066548(4)
$N = 74$	−0·066298(4)	$N = 69$	−0·066420(4)	$N = 80$	−0·066535(3)
$N = 114$	−0·066270(4)	$N = 113$	−0·066369(4)	$N = 120$	−0·066538(3)
E_∞^{VMC}	−0·066249(6)		−0·066345(6)		−0·066530(2)
b_1	0·0010(1)		0·0020(2)	c	−0·0063(4)
b_2	−0·0030(2)		−0·0032(4)		
χ^2	0·01		1·28		2·99
E_{58}^{DMC}	−0·06754(1)	E_{57}^{DMC}	−0·067473(8)	E_{56}^{DMC}	−0·06751(1)
E_∞^{DMC}	−0·06751(1)	E_∞^{DMC}	−0·06744(2)	E_∞^{DMC}	−0·06749(1)
E_c	−0·02861(1)		−0·01307(2)		

To date we have performed calculations for coupled layers of electrons at $r_s = 30$ and $d/r_s a_B = 0{\cdot}2, 0{\cdot}5, 1, 1{\cdot}5$. In fact we also have results for $r_s = \infty$ from the previous section. In Tables 6 and 7 we report our energies extrapolated to the bulk limits as obtained respectively from VMC and fixed-node DMC calculations. The DMC data are also illustrated in Fig. 6, where we compare the energy of the three phases that we have studied. It is evident that correlation indeed favours and stabilises the triangular crystal at intermediate distances $0{\cdot}5 \lesssim d/r_s a_B \lesssim 2{\cdot}0$, reverting the isolated layer situation, where the fully polarised liquid is still stable at this coupling, with the normal fluid having the largest energy. However for smaller distances, $d \lesssim r_s a_B$, it is the normal fluid that takes over the other two phases, favoured by the inter-layer screening (see below). We may mention that also the polarised fluid coupled layers will eventually become, for distances small enough for tunnelling to set in, lower in energy than the crystalline phase, as for $d = 0$ it becomes equivalent to a single unpolarised layer of double in-plane density.

Table 6. The VMC ground state energy (in Ry) in the bulk limit for two coupled electron layers at $r_s = 30$, as a function of the distance d, for three different phases

$d/r_s a_B$	Normal fluid	Polarised fluid	Triangular crystal
0·2	−0·075261(6)	−0·075037(7)	−0·075037(4)
0·5	−0·066249(6)	−0·066345(6)	−0·066530(2)
1·0	−0·063572(3)	−0·063859(4)	−0·063942(2)
1·5	−0·063322(3)	−0·063618(4)	−0·063664(2)

Table 7. The fixed-node DMC ground state energy (in Ry) in the bulk limit for two coupled electron layers at $r_s = 30$, as a function of the distance d, for three different phases

$d/r_s a_B$	Normal fluid	Polarised fluid	Triangular crystal
0·2	−0·07657(2)	−0·07627(1)	−0·07631(1)
0·5	−0·06751(1)	−0·06744(2)	−0·06749(1)
1·0	−0·06412(1)	−0·06420(1)	−0·064238(4)
1·5	−0·06384(1)	−0·06388(1)	−0·063900(6)

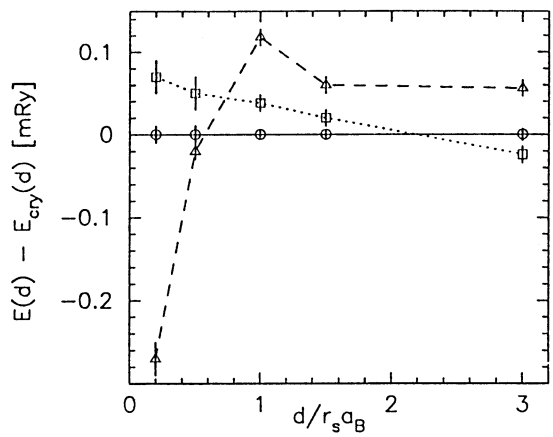

Fig. 6. Ground state energy of coupled layers of electrons at $r_s = 30$, as a function of the inter-layer distance d, in the normal and fully polarised fluid phases, referred to that of two crystalline layers in a triangular AB stacking (see text). Triangles, squares and dots refer respectively to the normal, fully polarised, and crystalline phase. Error bars are also shown. The lines are a guide to the eye.

We also have preliminary scattered results on coupled electron–hole layers at $r_s = 30$ and distances $d \lesssim r_s a_B$, but large enough to prevent both tunnelling as well as excitonic pairing (see, for instance, Lozovik and Yudson 1976). We again find a stabilisation of coupled crystalline layers with respect to the fluid phases. Clearly, in the presence of attraction between electrons and holes, we consider an AA stacking for the crystalline layers; that is, the second layer is displaced vertically from the first one without any in-plane translation.

(5b) Correlations

The study of pair correlations in coupled layers is interesting in its own right. Moreover, it gives further insight into the energetics of these systems. The pair correlation functions for two symmetric coupled layers a and b, of average in-plane density n_0, are conveniently defined by

$$g_{aa}(r) = \frac{1}{Nn_0} \sum_{i \neq j=1}^{N} \langle \delta(|\mathbf{r}_i^a - \mathbf{r}_j^a - \mathbf{r}|) | \rangle \,, \tag{36}$$

$$g_{ab}(r) = \frac{1}{Nn_0} \sum_{i,j=1}^{N} \langle \delta(|\mathbf{r}_i^a - \mathbf{r}_j^b - \mathbf{r}|) | \rangle \,. \tag{37}$$

As in the case of an isolated layer, we construct independently VMC and DMC pair correlations, and from these the extrapolated estimator.

We should emphasise that the above definition of the pair correlation functions is also applied to the crystalline phase, with an additional spherical average over the orientation of $\mathbf{r}$. This is quite common in all simulations studies. The relation with the pair correlation function usually encountered in the literature on non-uniform systems, $n^{(1)}(\mathbf{r}_1)n^{(1)}(\mathbf{r}_2)g(\mathbf{r}_1,\mathbf{r}_2) = n^{(2)}(\mathbf{r}_1,\mathbf{r}_2)$, is as follows. Within a proportionality factor, our averaged $g(r)$ is nothing but the average of $n^{(2)}(\mathbf{r}', \mathbf{r}'+\mathbf{r})$ over $\mathbf{r}'$ and the orientation of $\mathbf{r}$. Above, $n^{(1)}$ and $n^{(2)}$ are respectively the one- and two-body densities. Thus, the present definition mixes *intrinsic* pair correlations, described by $g(\mathbf{r}_1,\mathbf{r}_2)$, with the one-body order described by $n^{(1)}(\mathbf{r})$.

In Fig. 7 we give the pair correlations functions for coupled crystalline layers and fully polarised fluid layers, at a distance $d = 1{\cdot}5 r_s a_B$ and for $r_s = 30$. It is evident that in both cases the in-plane correlations are identical to those of an isolated layer, which are also shown. The inter-layer correlations are essentially absent [$g_{ab}(r) \simeq 1$ within error bar] for the polarised fluid. There appears to be a substantial amount of inter-layer correlation instead for the coupled crystals. However we should caution the reader that this is just an artifact of the present definition, which mixes one- and two-body order. We anticipate that, if one sampled $g(\mathbf{r}', \mathbf{r}'+\mathbf{r})$, one would find a structureless inter-layer function, as for the polarised fluid. Unfortunately $g(\mathbf{r}', \mathbf{r}'+\mathbf{r})$—or for what matters its average on $\mathbf{r}$ and the orientation of $\mathbf{r}$—is not easy to sample. To the best of our knowledge we are not aware of any computer simulation to date sampling $g(\mathbf{r}_1,\mathbf{r}_2)$, neither for classical nor for quantum systems.

In Fig. 8 we show the same functions as in Fig. 7, but for $d = 0{\cdot}2 r_s a_B$. The inter-layer correlations are now quite strong, and in fact appear to be much stronger than the in-plane ones for both cases considered. This increase of the inter-layer correlations is clearly at the expense of the in-plane ones which are depressed with respect to their value in the isolated layer. We have in fact results for $g_{aa}(r)$ and the $g_{ab}(r)$ also at the intermediate distances $d = r_s a_B$ and $d = 0{\cdot}5 r_s a_B$. We can draw the following conclusions: $g_{aa}(r)$ [$g_{bb}(r)$] remains essentially unchanged as the distance is decreased up to $d = r_s a_B$. For smaller distances one finds a progressive depression of in-plane correlations, and substantial enhancement of the in-plane tunnelling to small inter-particle separation. The $g_{ab}(r)$, on the

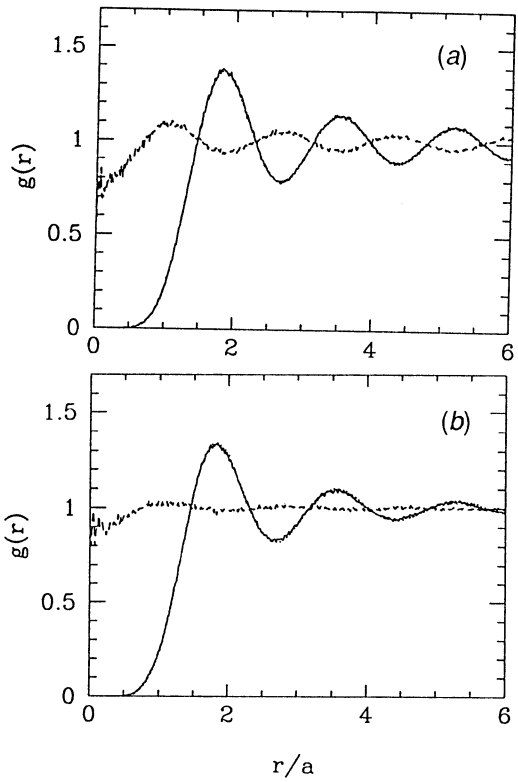

Fig. 7. Pair correlation functions in (a) two coupled crystalline layers with a triangular structure and an AB stacking (see text), and (b) two coupled fully polarised fluid layers, at $r_s = 30$ and $d = 1{\cdot}5 r_s a_B$. Full and dashed curves give respectively the in-plane and the inter-layer pair correlation function. The $g(r)$ of an isolated layer is indistinguishable from the full curve giving the in-plane pair correlation function.

other hand, becomes more and more structured with decreasing distance and its oscillations appear to be in anti-phase with those of $g_{aa}(r)$. Similar conclusions appear to be valid for the normal fluid coupled planes. For a more detailed discussion we refer the interested reader to Rapisarda and Senatore (1996).

The relations between the behaviour of pair correlation functions and that of the energy in the coupled layers systems should be now clear. The intrinsic two-body intra-layer correlations are negligible for distances larger than $r_s a_B$. Thus, at these distances the energy lowering in bringing together two planes should be larger for the crystalline phase, for which there is a *pre-existing* density modulation yielding a small though not negligible gain of (Hartree) potential energy. The picture changes as inter-layer correlations build up, at the expense of the intra-layer ones. This clearly disrupts the crystalline order, as is evident from Fig. 8a, eventually favouring the fluid phases.

6. Conclusions

We have presented an extensive state-of-the-art MC study of interacting electrons in two dimensions and in various phases for an isolated layer, as well

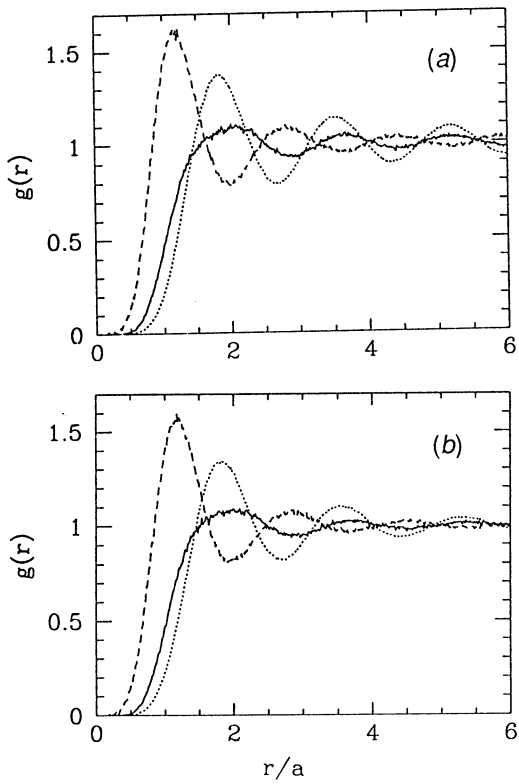

Fig. 8. Pair correlation functions in (a) two coupled crystalline layers with a triangular structure and an AB stacking (see text), and (b) two coupled fully polarised fluid layers, at $r_s = 30$ and $d = 0{\cdot}2r_s a_B$. Full and dashed curves give respectively the in-plane and the inter-layer pair correlation function. The $g(r)$ of an isolated layer is also shown for comparison (dotted curve).

as for two coupled layers at strong coupling and at various inter-layer distances. We have discussed in detail the phase diagram of the 2-dimensional electron gas and its pair correlation functions. Also, we have presented preliminary results for coupled electron layers, both for the energetics and the pair correlation functions, discussing how correlations yield a stabilisation of coupled crystals with respect to fluid phases. This is the first MC study on such a system and provides the most accurate information to date. We are currently extending our investigation to yield a more thorough mapping of the phase diagram and we are also systematically extending calculations to the problem of electron–hole coupled layers.

Acknowledgments

We would like to acknowledge invaluable discussions with Saverio Moroni on many aspects of the present work, as well as stimulating interactions with David Ceperley: he also developed the QMC code used in our study. David Neilson drew our attention to the problem of coupled layers, and stimulated it further with the invitation of one of us (GS) to Sydney. This work was supported in

part by MURST through the INFM. The calculations were mostly done on three DEC-alpha workstations belonging respectively to the INFM and INFN groups of the Dipartimento di Fisica Teorica.

References

Ando, T., Fowler, A., and Stern, F. (1982). *Rev. Mod. Phys.* **54**, 437.
Bednorz, J. G., and Müller, K. A. (1986). *Z. Phys.* **64**, 1175.
Bloch, F. (1929). *Z. Phys.* **57**, 549.
Bonsall, L., and Maradudin, A. A. (1977). *Phys. Rev.* B **15**, 1959.
Ceperley, D. M. (1978). *Phys. Rev.* B **18**, 3126.
Ceperley, D. M. (1991). *J. Stat. Phys.* **63** 1237.
Ceperley, D. M., and Kalos, M. H. (1979). In 'Monte Carlo Methods in Statistical Physics' (Ed. K. Binder), p. 145 (Springer: Berlin).
Eiseinstein, J. P., Pfeiffer, L. N., and West, K. W. (1992*a*). *Phys. Rev. Lett.* **68**, 674.
Eiseinstein, J. P., Pfeiffer, L. N., and West, K. W. (1992*b*). *Phys. Rev. Lett.* **69**, 3804.
Eiseinstein, J. P., Pfeiffer, L. N., and West, K. W. (1995). *Bull. Am. Phys. Soc.* **40**, 644.
Gaskell, T. (1961). *Proc. Phys. Soc. London* **77**, 1182.
Goldman, V. J., Santos, M., Shayean, M., and Cunningham, J. E. (1990). *Phys. Rev. Lett.* **65**, 2189.
Gupta, L. C., and Multari, M. S. (1993). 'Selected Topics in Superconductivity', Frontiers in Solid State Sciences **1** (World Scientific: Singapore).
Isihara, A. (1989). *Solid State Phys.* **42**, 271.
Jiang, H. W., Willet, R. L., Stormer, H. L., Tsui, D. C., Pfeiffer, L. N., and West, K. N, *et al.* (1990). *Phys. Rev. Lett.* **65**, 633.
Kwon, Y. (1994). private communication.
Kwon, Y., Ceperley, D. M., and Martin, R. M. (1993). *Phys. Rev.* **48**, 12037.
Liu, K. S., Kalos, M. H., and Chester, G. V. (1974). *Phys. Rev.* A **10**, 303.
Lozovik, Y. E., and Yudson, V. I. (1976). *Sov. Phys. JETP* **44**, 389.
March, N. H. (1958). *Phys. Rev.* **110**, 604.
Metropolis, N., Rosenbluth, A., Rosenbluth, M., Teller, A. H., and Teller, E. (1953). *J. Chem. Phys.* **21**, 1087.
Moroni, S., Ceperley, D. M., and Senatore, G. (1993). (unpublished).
Moroni, S., Fantoni, S., and Senatore, G. (1995). (unpublished).
Neilson, D., Świerkowski, L., Szymański, J., and Liu, L. (1993). *Phys. Rev. Lett.* **71**, 4035.
Overhauser, A. W. (1959). *Phys. Rev. Lett.* **3**, 414.
Overhauser, A. W. (1960). *Phys. Rev. Lett.* **4**, 462.
Overhauser, A. W. (1962). *Phys. Rev.* **128**, 1437.
Pudalov, V. M., D'Iorio, M., Kravchenko, S. V., and Campbell, J. W. (1993). *Phys. Rev. Lett.* **70**, 1866.
Rapisarda, F., and Senatore, G. (1996). (to be published).
Reynolds, P. J., Ceperley, D. M., Alder, B. J., and Lester, W. A. (1982). *J. Chem. Phys.* **77**, 5593.
Singwi, K. S., Tosi, M. P., Land, R. H., and Sjölander, A. (1968). *Phys. Rev.* **176**, 589.
Sivan, U., Solomon, P. M., and Shtrikman, H. (1992). *Phys. Rev. Lett.* **68**, 1196.
Świerkowski, L., Neilson, D., and Szymański, J. (1991). *Phys. Rev. Lett.* **67**, 240.
Tanatar, B., and Ceperley, D. M. (1989). *Phys. Rev.* B **39** , 5005.
Tsui, D. C., Störmer, H. L., and Gossard, A. C. (1982). *Phys. Rev.* **48**, 1599.
Umrigar, C. M., Wilson, K. G., and Wilkins, J. W. (1988). *Phys. Rev. Lett.* **60**, 1719.
Umrigar, C. J., Nightingale, M. P., and Runge, K. J. (1993). *J. Chem. Phys.* **99**, 2865.
von Klitzing, K., Dorda, G., and Pepper, H. (1980). *Phys. Rev. Lett.* **45**, 494.
Vosko, S. H., Wilk, L., and Nusair, M. (1980). *Can. J. Phys.* **58**, 1200.
Wigner, E. (1938). *Trans. Faraday Soc.* **34**, 678.
Williams, F. T. B., *et al.* (1991). *Phys. Rev. Lett.* **66**, 3285.
Zheng, L., and Fertig, H. A. (1995). *Bull. Am. Phys. Soc.* **40**, 197.
Zheng, L., and MacDonald, A. H. (1994). *Phys. Rev.* B **49**, 5522.

Manuscript received 19 June, accepted 7 August 1995